Photon asymmetry measurement in radiative muon capture on ^{40}Ca

A. Pouladdej,* T. P. Gorringe,† M. D. Hasinoff, A. J. Larabee,‡ A. J. Noble,§ C. J. Virtue,‖ and D. H. Wright¶
University of British Columbia, Department of Physics and Astronomy, Vancouver, British Columbia, Canada V6T 1Z1

G. Azuelos**
TRIUMF, Vancouver, British Columbia, Canada V6T 2A3

B. C. Robertson
Queen's University, Department of Physics and Astronomy, Kingston, Ontario, Canada K7L 3N6
(Received 6 January 2003; revised manuscript received 4 June 2003; published 5 September 2003)

A measurement of the photon asymmetry (α_γ) in radiative muon capture RMC on ^{40}Ca has been carried out at TRIUMF. Negative muons were stopped in a ^{40}Ca target and the resulting RMC photons were then converted by a 5-cm thick NaI detector placed immediately in front of our main NaI detector, a cylindrical crystal of diameter 46 cm and depth 51 cm. The data sample consisted of 5200 high-energy (57 MeV$<E_\gamma<$95 MeV) RMC photon candidates. Our measured value for the energy-averaged photon asymmetry is $\alpha_\gamma=1.00\pm0.23$. The extracted values for the induced pseudoscalar coupling constant (g_P) based on this photon asymmetry measurement are $g_P/g_A<8.0$, utilizing the impulse approximation IA model, and $g_P/g_A<14.5$ in terms of the modified impulse approximation (MIA) model. The two extracted values, although both consistent with the Goldberger-Treiman value of $g_P/g_A\approx7$, are considerably different, indicating a significant theoretical model dependency.

DOI: 10.1103/PhysRevC.68.034605 PACS number(s): 23.40.Bw, 25.40.Lw, 23.20.Nx

I. INTRODUCTION

The interest in weak interactions goes back to the early days of radioactivity where the weak force manifested itself through a common form of radioactivity, the β decay of nuclei for which the elementary processes are

$$n\rightarrow p+e^-+\overline{\nu}_e,$$

$$p\rightarrow n+e^-+\overline{\nu}_e.$$

The muon capture process ($\mu^-+p\rightarrow n+\nu_\mu$), a strangeness conserving semileptonic reaction, can be used as a powerful probe of nuclear structure, or, if the initial and final nuclear states are well known, it can then provide new information on the weak interaction due to the much higher momentum transfer (resulting from the larger muon mass). One fundamental parameter of interest investigated in such a probe is the pseudoscalar coupling constant of the weak interactions g_P. In the context of a nuclear capture process, the above muon capture reaction is referred to as ordinary muon capture (OMC). In the case of a ^{40}Ca target nucleus, one has

$$\mu^-+{}^{40}\mathrm{Ca}\rightarrow\nu_\mu+{}^{40}\mathrm{K}^\star.$$

This paper is concerned with a suppressed version of the above nuclear capture process known as radiative muon capture (RMC):

$$\mu^-+{}^{40}\mathrm{Ca}\rightarrow\nu_\mu+\gamma+{}^{40}\mathrm{K}^\star.$$

The small branching ratio for RMC compared to OMC,[1] makes the RMC process much less favorable and its observation much more difficult. However, due to the increased sensitivity of RMC to the induced pseudoscalar coupling constant, its study is of great interest. In fact, OMC and RMC provide the two main sources of information for g_P determination.

In nuclear muon capture experiments some possible observables are the total capture rate, polarization, asymmetry, and energy distributions of the emitted nucleons. With RMC experiments, different aspects associated with the emitted photons are of interest and the most frequently measured quantities in such experiments are the partial branching ratio and photon asymmetry α_γ. In the case of RMC for a polarized μ^- beam, the *parity violation* of the weak interaction is manifested as an angular correlation between the direction of emission of RMC photon and the direction of polarization of μ^-. The observed angular distribution or ''yield'' for RMC photons is given by

*Present address: Nortel Networks, Advanced Technology Division, Ottawa, Ontario Canada K2H 8E9.
†Present address: University of Kentucky, Department of Physics, Lexington, Kentucky 40506, USA.
‡Present address: Greenville College, Department of Physics, Greenville Illinois 62246, USA.
§Present address: Queen's University, Department of Physics, Kingston, Ontario, Canada, K7L 3N6.
‖Present address: Laurentian University, Department of Physics and Astronomy, Sudbury, Ontario, Canada, P2E 2C6.
¶Present address: Stanford Linear Accelerator Center, Menlo Park, California 9405, USA.
**Also at Université de Montréal, Montréal, Quebec, Canada, H3C 3J7.

[1]The ratio of RMC to OMC rate is $(\Lambda_{\mathrm{RMC}}/\Lambda_{\mathrm{OMC}})\approx2\times10^{-5}$.

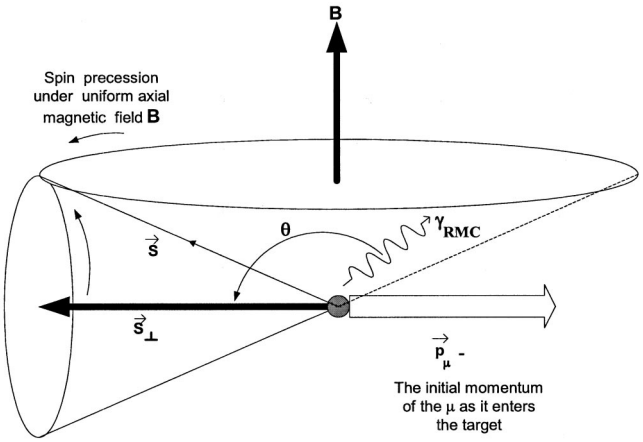

FIG. 1. The schematics of RMC photon angular emission: $\vec{p}_{\mu^-}$ is the muon's initial linear momentum as it enters the target, $\vec{s}_\perp$ is the μ^- spin-quantization axis, and $\vec{s}$ is the actual μ^- spin. It is emphasized that μ^- capture in the target occurs at rest, the direction as indicated by $\vec{p}_{\mu^-}$ is that of μ^- as it enters the target.

$$Y_\gamma(\theta)=N_\gamma[1+(\langle P_{\mu^-}\rangle\alpha_\gamma)\cos\theta]=N_\gamma[1+A_\gamma\cos\theta], \tag{1}$$

where $Y_\gamma(\theta)$ is the angular yield, which is the rate of emission of RMC photons for the given polar angle θ—this is the angle between the direction of emission of RMC photon and the μ^- spin-quantization axis, N_γ is a normalization factor, A_γ is the magnitude of ''observed'' or ''measured'' photon asymmetry, α_γ is the ''energy-averaged'' or the ''physical'' photon asymmetry, and $\langle P_{\mu^-}\rangle$ is the average μ^- beam spin-polarization before capture, see Fig. 1. The V-A theory predicts 100% right circularly polarized photons, so for a pure V-A theory $\alpha_\gamma=+1$ exactly.

In order to better understand how the pseudoscalar coupling constant fits into the weak interaction picture, we can consider the weak interaction Hamiltonian for the muon caputre in terms of the four fermion coupling and the Gell-Mann-Cabbibo universality [1,2]:

$$H_w=\frac{G\cos\theta_c}{\sqrt{2}}\overline{\psi}_n(V_\lambda+A_\lambda)\psi_p\overline{\psi}_\nu\gamma_\lambda(1+\gamma_5)\psi_\mu+\text{H.c.}, \tag{2}$$

where ''G'' is the Fermi coupling constant[2] and ''θ_c'' is the Cabbibo mixing angle. The ψ_ξ's are the spinor functions for the fermions $\xi=n,\ p,\ \nu$, and μ. The phenomenological forms of the hadronic vector and axial vector terms are given by

$$V_\lambda=g_V\gamma_\lambda-\left(\frac{g_M}{2m_N}\right)\sigma_{\lambda\rho}q^\rho-\left(\frac{ig_S}{m_\mu}\right)q_\lambda,$$

$$A_\lambda=g_A\gamma_\lambda\gamma_5-\left(\frac{ig_p}{m_\mu}\right)q_\lambda\gamma_5-\left(\frac{g_T}{2m_N}\right)\sigma_{\lambda\rho}q^\rho\gamma_5.$$

[2]The value of $G\cos\theta_c=(1.41220\pm0.00043)\times10^{-49}$ erg cm^3 [3].

The four-momentum transfer is given by $q_\lambda=n_\lambda-p_\lambda$, where n_λ and p_λ are the neutron and proton four-momenta, m_N and m_μ are the nucleon and muon masses, respectively. The parameters g_V, g_M, g_S, g_A, g_P, and g_T are the basic ''coupling constants'' for the semileptonic interaction. The coupling constants g_M, g_S, g_P, and g_T are ''induced'' by the strong interactions of the hadrons. The main component of the pseudoscalar coupling g_P is the one pion exchange diagram with a propagator $1/(m_\pi^2-q^2)$, where m_π is the mass of the charged pion. In OMC, the four-momentum transfer is fixed at $q^2=-0.88m_\mu^2$, while in the case of RMC a value of $q^2\approx m_\mu^2$ is achievable near the maximum photon energy, thereby enhancing the amplitude of the one pion exchange contribution by a factor of ~3. Consequently, the pseudoscalar coupling, which is absent in the β decay and affects OMC very little, strongly influences the high energy part of the photon energy spectrum and the absolute rate for RMC. The identification of this strong dependence of the total rate of the photon energy spectrum on g_P was the initial motivation for the experimental study of RMC. The very low rate ($R_{k>57\text{ MeV}}\sim2\times10^{-5}$) for RMC favored rate measurements on heavy nuclei. For these nuclei the Coulomb attraction concentrates the muon's wave function over the nuclear volume, effectively increasing the capture rate. However, with heavier nuclei, many theoretical difficulties arise. To reduce such effects doubly magic nuclei such as ^{16}O and ^{40}Ca with relatively simple nuclear structure have been favored both for theoretical considerations and experimental investigations.

The partially conserved axial current (PCAC) formulation allows an estimation of g_P for a ''free'' nucleon—g_P is believed to be a very robust prediction based on our understanding of the manifestation of approximate chiral asymmetry. This leads of the well-known Goldberger-Treiman expression [4]:

$$g_P(q^2)=\frac{2m_\mu m_N}{m_\pi^2-q^2}g_A(0), \tag{3}$$

which results in the value of $g_P(-0.88m_\mu^2)=6.77g_A(0)=8.58$ [5]. By comparing the experimentally determined value of g_P with the Goldberger-Treiman value, it is then possible, at least in principle, to draw conclusions about the possible renormalization of g_P within nuclear matter [6].

II. THEORETICAL BASIS

It is generally accepted that QCD is the fundamental theory of strong interactions although it cannot be readily applied at low energies. In order to investigate interactions at the quark-lepton level one must rely on a phenomenological description of the weak interactions. The Standard Model of the weak interactions, as seen in Eq. (2), describes such interactions in terms of fundamental coupling constants that need to be determined experimentally. The vector and weak magnetism coupling constants $g_V(q^2)$ and $g_M(q^2)$ are related by the conserved vector current (CVC) theory to the electromagnetic current [7] and have been measured by elec-

tron scattering. The scalar and tensor coupling constants $g_S(q^2)$ and $g_T(q^2)$ are predicted to be absent due to G-parity invariance and this is consistent with experimental measurements [8,9]. The axial vector coupling constant $g_A(q^2)$ can be determined accurately from neutron β decay [3] and its q^2 dependence from neutrino scattering [10], or pion electroproduction [11,12]. This leaves the induced pseudoscalar coupling constant $g_P(q^2)$ which is by far the least well known of these coupling constants.

A. Muon capture on hydrogen and the "g_P Puzzle"

Recent developments in QCD in terms of chiral perturbation theory (ChPT) have provided an appropriate field theory for low-energy interactions. The heavy baryon chiral perturbation theory (HBChPT) [13,14], which is a specific form of ChPT useful when nucleons are involved, has allowed theoretical formulations to go beyond the PCAC approach. Calculations in the context of the HBChPT approach [15,16] have provided a rigorous justification for the Goldberger-Treiman estimate and Adler-Dothan correction [4] to yield a modified expression for g_P as follows:

$$g_P(q^2)=\frac{2m_\mu g_{\pi\mathrm{NN}}(q^2)F_\pi}{m_\pi^2-q^2}-\frac{1}{3}g_A(0)m_\mu m_N r_A^2, \qquad (4)$$

where $g_{\pi\mathrm{NN}}$ is the pion-nucleon coupling constant, r_A is the nucleon axial radius, and F_π is the pion decay constant. Equation (4) leads to a predicted value of $g_P(-0.88m_\mu^2)=8.70-0.45=8.25$ [5]. Comparing results from Eqs. (3) and (4) reveals that the correction term for g_P is rather small. Furthermore, in the above $O(q^3)$ HBChPT formulation, the Goldberger-Treiman term appears as the first term of the chiral series expansion. The value of g_P determined by Bardin et al. For OMC reaction on hydrogen [17] is in good agreement with the PCAC prediction. However, somewhat surprisingly, the TRIUMF results for RMC on hydrogen [18,19] yield a value for g_P, which is $\sim$1.5 times larger than the PCAC prediction! Furthermore, the HBChPT calculation up to next-to-next-to-leading order (NNLO) [20] shows that the chiral series converges rapidly. This indicates that the discrepancy between experiment and theory for RMC on hydrogen cannot be explained by higher order perturbation corrections within the context of HBChPT [21].

B. Muon capture on heavy nuclei

The first theoretical attempt at evaluating the total capture rate for nuclei was carried out by Wheeler [22]. He assumed that the capture rate was proportional to the overlap of the muon wave function at the nucleus and obtained the classical prediction of $\Lambda_c \propto Z_{\mathrm{eff}}^4$, where Z_{eff} is an effective charge for the nucleus. For light nuclei $Z_{\mathrm{eff}} \sim Z$.

Subsequent theoretical advancements since then have been based on two general approaches, the impulse approximation (IA) and the elementary particle approach (EPA). It has been pointed out that the EPA in its present form lacks serious justification and is insufficient for two step processes such as RMC [23,24]. As a result, the majority of the calculations pertaining to RMC have employed the IA. There are basically three different models for treating RMC within the framework of the standard IA. *Closure models*: These are the simplest models and are based on nuclear sum rules and they assume that all of the existing nuclear final states are attainable. *Phenomenological models*: For these models a phenomenological nuclear response function is proposed, which divides the transition strength into a dipole and a quadrupole part.[3] One instance of such a model was developed by Christillin [25], who has criticized closure models purely on theoretical grounds. He argued that the closure sums include states of nuclear excitation, which are energetically forbidden. As the RMC photon energy increases, the allowed part of the excitation energy decreases. This explains why all closure models overestimate RMC rates. *Microscopic models*: The approach taken in the case of these models, developed by Gmitro *et al.* [26], is to employ detailed wave functions for the initial and all the important final nuclear states and then perform a detailed microscopic calculation summed over all partial transitions. This technique also suffers from an overestimation of RMC rates.

TABLE I. The energy-averaged (with the energy cutoff of $E_\gamma > 57$ MeV) photon asymmetries for ^{40}Ca as calculated by several different models, using the Goldberger-Treiman value for g_P.

α_γ	Reference
0.75	Rood and Tolhoek [28]
0.78	Rood, Yano, and Yano [29]
0.76	Sloboda and Fearing [30]
0.79	Christillin (Phenomenological Model) [25]
0.77	Gmitro *et al.* (IA) [26]
0.95	Gmitro *et al.* (MIA) [27]

Table I shows α_γ values, which are energy-averaged photon asymmetries with the energy cutoff of $E_\gamma > 57$ MeV, for ^{40}Ca evaluated based on several different models, using the Goldberger-Treiman value for g_P. The last entry in the Table I is based on the MIA approach proposed by Gmitro *et al.* [27], which is significantly different than the predictions based on other traditional models. The MIA model was developed in order to account for the discrepancy between the photon yield as predicted by the phenomenological model of Christillin [25] and the earlier IA model of Gmitro *et al.* [26]. They applied meson exchange corrections (MEC) to their IA technique by introducing constraints imposed by the electromagnetic continuity equation at the pion vertex. These MEC corrections resulted in a reduction of the rate by almost a factor of 2 for ^{40}Ca. However, it should be pointed out that although the MIA is quite successful in predicting RMC rates, it predicts a lower sensitivity of α_γ to g_P and this is a sharp departure from the "model independence of α_γ versus g_P" as predicted by the earlier theoretical work.

[3]In the phenomenological models, the dipole strength is fixed from related electroweak data and the quadrupole strength is fixed by OMC.

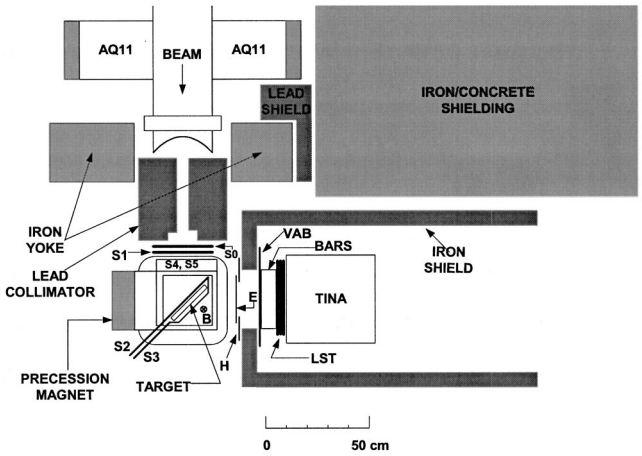

FIG. 2. Detailed design of the experiment including the shielding plan in the vicinity of M20A beamline to guard against background radiation for RMC ^{40}Ca experiment at TRIUMF.

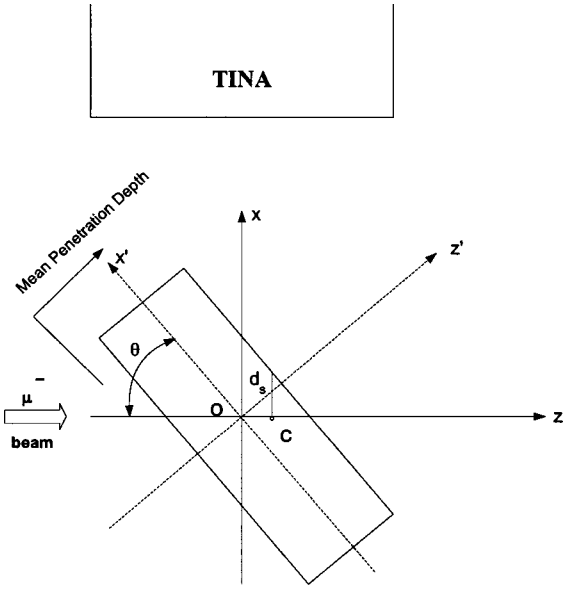

FIG. 3. Target setup (not to scale). *C* is the centriod of the stopping distribution, *o* is the geometrical center of the compound target, *x* indicates the direction of the photon telescope, *z* is the direction of the incident beam, and d_s is the ''emergence length,'' which is measured from the centroid of the stopping distribution to the back face of the target in a direct line towards TINA. The primed axes $x'y'z'$ are a planar rotation—in the (x,z) plane—of the x,y,z axes by the angle θ.

III. GENERAL EXPERIMENTAL ASPECTS

The experimental data presented in this paper were obtained by using the backward μ^- beam from the M20A channel at TRIUMF. The data were collected at two different average beam momenta of 76 MeV/*c* and 86 MeV/*c*. The experiment was designed in the manner of a muon spin rotation (μSR) experiment [31]. The μSR technique relies on the fact that a muon decays preferentially along its helicity direction—this was exploited in the following manner. The muon beam entered the experimental area with its polarization vector[4] essentially longitudinal and it was then allowed to strike a target situated in a uniform transverse magnetic field. For those muons that were stopped within the target, the magnetic field caused their spins to precess in a horizontal plane at a uniform rate, see Fig. 1. By observing the RMC photons in a stationary detector placed at a fixed angle to the direction of the incident μ^- beam, the photon asymmetry manifested itself as a periodic time component superimposed upon a normal exponential decay curve in the resulting time spectrum.

A. Experimental setup

The key features of the geometrical setup of the experiment are shown in Fig. 2, where the main detection component was the photon telescope (TINA + BARS). The whole setup was completely covered with large blocks of concrete to provide an effective shielding against the unwanted background radiations. The backgrounds encountered in this experiment can be categorized into three main classes: cosmic rays, beam or cyclotron-related, and target-associated. Neutrons and cosmic rays were a very major source of background contamination in this experiment. Consequently, shielding against such unwanted events was a major design consideration. Without any shielding, the RMC photons were detectable with a signal-to-noise ratio of 0.5 to 1, while with the added shielding we achieved a signal-to-noise ratio of 7 to 1.

The target: It consisted of two geometrically identical slabs of natural calcium (97% ^{40}Ca) protected by a thin coating of aluminum. The target was designed with two conditions in mind: first, to have as large a fraction of the incident muon's stop in the target as possible; second, to have the centroid of the stopping distribution as close as possible to the back face of the target in direct view of TINA. This latter requirement was necessary in order to reduce the bremsstrahlung radiations arising from decay electrons within the target, and thereby allowing a better determination of the μ^- beam polarization before capture by reducing the Monte Carlo (MC) dependence of our result. The distance parameter used in the above minimization was the ''emergence distance'' d_s, which was measured from the centroid of the stopping distribution to the back face of the target in a direct line towards TINA. Figure 3 shows the relevant geometry. The results of our MC simulation indicated that with our given set of experimental conditions of $\langle P_{\mu^-}\rangle = 76$ and 86 MeV/*c*, possible target inclination range $20° < \theta < 60°$, and a magnetic field of 0.041 T, the μ^- mean penetration depth varied from 0.7 to 1.6 cm (i.e., well within the thickness of one target slab). It was, therefore, decided to employ a ''thin-

[4]Due to the precession of a muon's spin in the bending magnets, the beam's polarization vector is not exactly longitudinal. The average value of polarization for μ^- beam and μ^+ beam in the M20A channel have been measured [32], and the average *residual* polarization for μ^- beam stopped in our ^{40}Ca target has been determined to be $\langle P_{\mu^-}\rangle = 0.111 \pm 0.010$.

TABLE II. Target inclination optimization results based on our Monte Carlo simulation studies.

	76 MeV/c		86 MeV/c	
$\theta°$	% stop in target	d_s (cm)	% stop in target	d_s (cm)
40	65	0.9	26	0.5
30	68	1.2	53	0.6
20	69	1.4	67	1.1

extended'' target obtained by placing the slabs end to end, resulting in a compound target size of 20 cm$\times$10 cm $\times$1.9 cm. An inclination angle of $\theta=30°$ was used, a choice that provided an acceptable level for both of the aforementioned requirements, see Table II. The Monte Carlo results for the % stops in the target values of 68% and 53% were in good agreement with the experimentally measured values of (70 ± 3)% and (53 ± 3)%, respectively.

The precession magnet: The desired magnetic field was obtained from a small *C* magnet, which provided a field homogeneity of 3% across the target. Its square pole faces measured 25.4 cm$\times$25.4 cm and were separated by a uniform gap of 15.2 cm. These pole faces were completely covered with 0.32 cm thick sheets of lead, so that any muon that missed the target would stop in lead rather than iron, and this would then produce a much faster decay background time component (for lead $\tau_{\mu^-}\approx75$ ns as compared to iron $\tau_{\mu^-}\approx142$ ns). The target, sandwiched between the two detectors $S2$ and $S3$, was then placed between the magnet's pole faces such that its geometrical center coincided with that of the gap. It had its cross-sectional plane of 20 cm$\times$10 cm vertical and was situated at 30° to the direction of the incident beam, see Fig. 3. The precession magnetic field had a nominal value of 0.041 T, resulting in a precession frequency of 5.5 MHz. Like an earlier TRIUMF experiment [32], it was decided not to employ the stroboscopic μSR method [33] in which the muon precession frequency is tuned to be equal to the cyclotron frequency.

Detection requirements: The detection task for this experiment consisted of the following: (i) identifying the arrival time and the ultimate fate of the incident muon, (ii) selecting the relevant events (charged or neutral) arising from the absorption or decay of the muon, and (iii) recording the time and energy information for each event.

Energy calibration: The active NaI converter (BARS) was calibrated by allowing a μ^+ beam of known energy to be incident directly on each element of this segmented detector. The larger total energy detector TINA was calibrated using the well-known photon spectrum from at-rest π^- capture in a H_2 gas target (i.e., π^-+p reaction). For this calibration, the ^{40}Ca target and its associated counters $S2$ and $S3$ were replaced with a high pressure (100 atmosphere) H_2 gas target. A full description of this H_2 gas target is given in Ref. [34]. The actual energy response function for the TINA is shown in Fig. 4. This observed spectrum results from convolution of the finite resolution of TINA with the ''ideal''

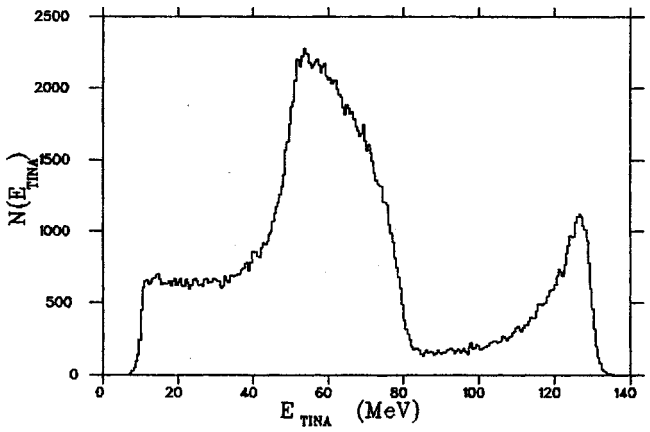

FIG. 4. The TINA energy spectrum from at-rest π^- capture in a H_2 gas target.

spectrum[5] having a monoenergetic line at 129 MeV and a flat-box spectrum between 55 and 83 MeV. It should be pointed out that the energy-measuring component of our experimental setup consisted of a calorimeter TINA and an active converter BARS. This configuration was favored over an only-calorimeter alternative, as it provided superior OMC neutron-discriminating capability for our setup. Unfortunately, the downside to this was that the presence of the BARS degraded our overall energy resolution—in fact, the rather large low-energy tail seen in TINA's observed energy spectrum is due to the BARS. This issue is further discussed in Sec. IV F in relation to DiLella *et al.*'s [35] experimental setup, which employed only a ''bare'' NaI detector without an active converter.

The beam counters: $S0-S5$ plastic scintillators were used to detect the arrival of a muon and its stoppage or passage through the target, see Fig. 2. $S4$ and $S5$ covered the pole faces of the magnet and in conjunction with $S2$ and $S3$ they formed a well-defined volume, which enclosed the target. These detectors experienced rates of the order of 400 kHz for μ stop events and had resolving times down to 5 ns.

The photon telescope: This was the most important part of the detector, as it measured the bulk of the RMC photon energy used in the construction of the neutral time spectrum from which we extracted the photon asymmetry. The ''telescope'' consisted of three main components.

(1) Charged particle identification was done via three plastic scintillators, E, H, and VAB: the VAB counter, a 58.0 cm$\times$48.0 cm$\times$0.32 cm veto counter rejected charged particles emitted by the target; the E counter, a 12.7 cmφ $\times$0.32 cm electron counter identified the decay electrons; the H counter, a 38.1 cm$\times$38.1 cm$\times$0.64 cm counter with a central hole of diameter of 15.2 cm rejected bremsstrahlung radiation resulting from the decay electrons hitting the lead collimator.

[5]The 129.4 MeV photon-peak is due to the single photon in the reaction $\pi^-+p\rightarrow n+\gamma$. On the other hand, the flat box also know as the π^0 box arises due to the detection of photons from π^0 decay in the nuclear process $\pi^-+p\rightarrow n+\pi^0\rightarrow\gamma+\gamma$.

(2) The photon energy measurement was performed via the two NaI (TI) detectors, TINA and BARS. TINA was a cylindrical crystal of diameter 46 cm and depth 51 cm enclosed in an aluminum container. It collected the electromagnetic showers that resulted from converted photons within the BARS. Because of its comparatively large geometrical volume, it absorbed most of the energy associated with a given neutral event. It had an energy resolution of 7.1% full width at half maxium (FWHM) for 129 MeV photons. The BARS detector consisted of seven geometrically identical, optically isolated blocks of NaI (TI)—each individual block measured 5.08 cm$\times$4.35 cm$\times$35.56 cm. This served as our γ converter, turning photons into electron-positron pairs. It had an energy resolution of 3.2% for 40 MeV pions. The photon telescope had an overall γ energy resolution of $\sim$15% FWHM at 70 MeV. By requiring simultaneous energy deposition $>$5 MeV in both the TINA and BARS, it was possible to discriminate against a considerable part of the neutron background, arising from OMC in the target as well as other background sources.

(3) Three 38.1 cm$\times$38.1 cm$\times$0.32 cm optically isolated plastic scintillators (LST 1,2,3) were used to help identify electrons, resulting from photon conversion in the BARS. Due to the rather poor energy resolution and efficiency the actual measured LST energy was not used in the off-line analysis—rather an average energy loss was substituted.

The observed event rates in the NaI and other veto counters were of the order of 500 Hz. The entire photon telescope was then placed in a 10-cm thick iron plate shielding box, which had a 30-cm diameter hole in its front face.

The cosmic-ray counters: To discriminate against cosmic rays, two additional sets of large plastic scintillators were used to cover the whole of the photon telescope. The ''inner'' counters were placed over and on both sides of TINA, while the ''outer'' counters were placed on the outside of the shielding box. These counters were used to identify cosmic-ray events that passed through or stopped in our apparatus.

The signals from the counters were processed by standard NIM modules and the relevant data were then passed via CAMAC to a computer for recording on magnetic tapes.

B. Logic and event selection

Three event categories were deployed.

(1) Neutral (NEU) events: A NEU event was intended for classifying those processes that were recognized as being electrically neutral at their point of creation inside the target. Examples were RMC and bremsstrahlung photons and OMC neutrons.

(2) Charged (CHG) events: A CHG event referenced charged decay electrons or positrons arising from muon decay in orbit. The CHG and NEU events were further combined logically to produce the more general ''good event'' (GDV).

(3) Pulser (PULSER) events: A PULSER event was obtained by using a beam pulser to sample events at random, following the arrival of a beam particle, thereby allowing the determination of the ''pedestals'' on our ADC's (i.e., providing information about the noise level on the counters as well as the thresholds of the ADC's).

In order to guard against muon stop events in the pole faces of our precession magnet, an associated inhibit signal was used. This inhibit signal was defined as an OR of the computer busy signal and a 300-ns-long signal of the form $[(S0+S1)\cdot(S4+S5)]$. The coincidence $(S0\cdot S1\cdot S2)$ signaled the arrival of a muon inside the target and $[S0\cdot S1\cdot S2\cdot(S3+S4+S5)]$ indicated that the muon had, in fact, stopped within the target. The elementary events were then defined as follows:

$$\mathrm{NEU}=\mathrm{TINA}\cdot\mathrm{BARS}\cdot\overline{\mathrm{NEUV}},$$

$$\mathrm{CHG}=\mathrm{BARS}\cdot S3\cdot E\cdot(\mathrm{VA}+\mathrm{VB})\cdot\overline{\mathrm{CHGV}},$$

$$\mathrm{GDV}=(\mathrm{NEU}+\mathrm{CHG})\cdot\overline{\mathrm{inhibit}},$$

$$\mathrm{PULSER}=S0\cdot S1\cdot S2\cdot\mathrm{beam\ pulser}\cdot\overline{\mathrm{inhibit}}.$$

The charged and neutral ''vetoes'' were defined as $\mathrm{CHGV}=S0+S1+H+\mathrm{charged\ pulser}$,[6] and $\mathrm{NEUV}=S0+S1+H+\mathrm{VA}+\mathrm{VB}$.[7]

The CAMAC modules were read out for both GDV and PULSER events. The decay of a captured muon within the target was observed within a 2-μs-long time window. If within the 2-μs time window a second (or third, etc.) muon arrived, that particular event was discarded.

IV. EXPERIMENTAL ANALYSIS

The RMC asymmetry measurements were carried out with a backward μ^- beam at two different average beam momenta of 76 and 86 MeV/c. The calibration data for TINA were obtained with a 100 MeV/c π^- beam, while the BARS were calibrated in an 86 MeV/c backward μ^+ beam.

A. The observable, α_γ

The energy-dependent RMC photon angular distribution is given by

$$W_\gamma(k,\theta)=1+\Gamma_\gamma(k)\cos\theta,$$

where $k\equiv E_\gamma$ is the photon energy, θ is the angle between the emitted RMC photon and the direction of the spin-quantization axis of μ^-, and $\Gamma_\gamma(k)$ is the energy-dependent photon asymmetry coefficient, which was defined in terms of the RMC rate (Λ_{RMC}) as follows:

$$\Gamma_\gamma(k)=\frac{(d\Lambda^+{}_{\mathrm{RMC}}/\mathrm{dk})-(d\Lambda^-{}_{\mathrm{RMC}}/\mathrm{dk})}{(d\Lambda^+{}_{\mathrm{RMC}}/\mathrm{dk})+(d\Lambda^-{}_{\mathrm{RMC}}/\mathrm{dk})},$$

where $\Lambda^+{}_{\mathrm{RMC}}\equiv\Lambda_{\mathrm{RMC}}(k,\theta=0)$ and $\Lambda^-{}_{\mathrm{RMC}}\equiv\Lambda_{\mathrm{RMC}}(k,\theta=\pi)$. Due to the low rate associated with RMC, an energy-dependent measurement of the photon asymmetry was not

[6]Due to the very large number of charged events, a random pulser known as the ''charged pulser'' was used to reduce (by a factor of $\sim$15) the rate at which charged events were recorded onto magnetic tapes.

[7]It is noted that the veto counter VAB had two wave-shifter bars one on each side. VA and VB refer to the signals from these two wave-shifter bars.

experimentally feasible. Furthermore, below 57 MeV, the experimental RMC energy spectrum was overpowered by bremsstrahlung photons, thus restricting the range over which the RMC could be accurately measured. Consequently, α_γ was defined over the experimentally accessible region of $k \geqslant 57$ MeV as

$$\alpha_\gamma = \frac{\int_{k>57\ \mathrm{MeV}} \Gamma_\gamma(k)\Lambda_{\mathrm{RMC}}\ \mathrm{dk}}{\int_{k>57\ \mathrm{MeV}} \Lambda_{\mathrm{RMC}}\ \mathrm{dk}}.$$

For 100% polarized μ^- before capture (experimentally not realizable), the angular distribution of the emitted RMC photons in terms of α_γ is then given by

$$W_\gamma(\theta) = 1 + \alpha_\gamma \cos\theta,$$

which is to be compared with Eq. (1).

B. Choice of the fitting function

The most general function describing the observed neutral time spectrum for this experiment has the form

$$\begin{aligned} N(t) &= \sum_i [N_i(t)] + B(t) \\ &= \sum_i \{N_{0i} e^{-t/\tau_i}[1 + A_{\gamma i}\cos(\omega t + \varphi) e^{-r_i t}]\} + B(t) \\ &= \sum_i \{N_{0i} e^{-t/\tau_i}[1 + A_{\gamma i}(t) e^{-r_i t}]\} + B(t), \end{aligned}$$

where the index "i" is to run over all the possible sources radiating the RMC photons. $N_i(t)$: number of events per unit time at time t for source i; number of events per unit time at time $t=0$ for source i; τ_i: decay lifetime of μ^- in source i material (e.g., $\sim$333.0 ns in ^{40}Ca); ω: angular precession frequency dictated by the magnetic field; φ: initial phase angle which is $\pm 90°$ for $\mu^\pm$ in this experiment; $B(t)$: time-dependent background term; $A_{\gamma i}$: magnitude of RMC photon asymmetry for source i; $A_{\gamma i}(t)$: time-dependent RMC photon asymmetry function for source i; r_i: relaxation parameter for source i.

The exponential term e^{-t/τ_i} arises because of the finite lifetime for the muon capture process. The periodicity inherent in the neutral time spectrum, which is associated with the precession of μ's spin, is expressed by $\cos(\omega t + \varphi)$. Any possible nonhomogeneity in the precession magnetic field will manifest itself through a relaxation of the signal and this is accounted for by the relaxation term $e^{-r_i t}$.

The main source of the RMC photons was the calcium target. There were two other minor sources that also contributed: the lead and the carbon components arising from μ^- absorption in the lead sheaths and the scintillators or their wrapping. From a two-component fit to the neutral time spectrum, it was determined that within the existing error bounds for this experiment the above two minor sources could be omitted from the fits without affecting the estimated value of the observed asymmetry for ^{40}Ca.[8] Furthermore, no relaxation effects were observed.[9] Hence the value of the observed asymmetry is independent of $t=0$. With these simplifications, the fitting function becomes a single time component equation, and takes the form of a standard μSR fitting function:

$$\begin{aligned} N(t) = N_{\mathrm{Ca}}(t) &= N_0 e^{-t/\tau}[1 + A_\gamma \cos(\omega t + \varphi)] + B(t) \\ &= N_0 e^{-t/\tau}[1 + A_\gamma(t)] + B(t). \end{aligned} \quad (5)$$

The quantity of interest is the physical photon asymmetry (α_γ). This was obtained by normalizing the observed photon asymmetry to the average residual μ^- beam polarization before capture, using Eq. (1). A χ^2 minimization was then carried out using the nonlinear functional-minimization program MINUIT [36]. The asymmetrical errors quoted for the estimated parameters are those provided by the MINOS subroutine that provides 1σ errors (i.e., 68% confidence limit).

C. Brief discussion of cuts and energy reconstruction for the RMC photons

The raw data were initially cleaned up with two cuts, one hardware and the other a software cut, before being subjected to any systematic analysis. These cuts were as follows.

(1) The neutron removal condition consisted of requiring >25 MeV total energy deposition in the TINA and the BARS, i.e., (BARS+TINA)>25 MeV in conjunction with the requirement [(BARS>5 MeV)$\cdot$(TINA>5 MeV)]. This latter condition was used since neutrons typically deposited energy in both the TINA and BARS simultaneously. This was a hardware cut applied by the data acquisition system; it was quite successful in removing the prolific neutron background. It discriminated against neutron background by a factor of >100.

(2) The low-energy neutral events were further removed by requiring >45 MeV total energy deposition in the TINA and the BARS. This was a software cut applied offline to produce the final "skimmed" data sample used in our analysis.

The 2-μs μ^- decay time window was divided into two distinct time regions, a foreground region, which was 985 ns long, and an early-time background region 1015 ns long. These two regions were separated by the "prompt peak," which had a full width $\sim$20 ns and signaled the arrival of a μ^- in the target region. The following software cuts were then applied to our skimmed data sample to construct our clean neutral time spectrum.

(1) *The prompt cut*: This cut was used to discard events that were prompt-in-time with a μ^- arrival. This was achieved by inspecting the S2 TDC and the S0+S1 pulse separator TDC's. This cut aimed at removing the π^--related background and its associated 43.37 ns cyclotron-related time structure.

[8] Both of these minor sources had very low contributions: $(N_{0\mathrm{Pb}}/N_{0\mathrm{Ca}}) \sim 10^{-6}$, $(N_{0C}/N_{0\mathrm{Ca}}) \sim 10^{-3}$.

[9] The relaxation term was found to be negligible $r_{\mathrm{Ca}} \sim 10^{-5}$.

(2) *The cosmic-ray cut*: It removed any events that were preceded by the passage of a cosmic ray through the apparatus as far back as 8 μs prior to the prompt timing for the event. This long veto was necessary in order to discriminate against any cosmic-ray μ's which stopped near TINA. It relied on the (IN•OUT) signal from the IN and OUT cosmic-ray counters to achieve this purpose.

(3) *The* 2^{nd} μ*-stop cut*: It rejected those events that occurred as a result of there being more than one μ-stop at a time in the target.

(4) *The bremsstrahlung cut*: This cut guarded against bremsstrahlung radiation arising from the interaction of the decay electrons inside the target and/or within the *C*-magnet pole faces; this was achieved by using the $S3$, $S4$, and $S5$ TDC's and their respective ADC's.

(5) *The layered scintillator cut*: It was the most successful cut in removing background. This cut placed a low- and a high-energy requirements on the LST's three elements. The ''low-energy'' cut was employed to identify a ''firing'' in any of the LST 1,2,3—it set the minimum energy deposition required in the LST's before an event was to be accepted. The ''high-energy'' cut discriminated against high-energy cosmic rays passing through the LST's.

For a more detailed discussion of these cuts, the reader is referred to Refs. [37,38].

The sum of the energies deposited in the BARS, TINA, LST and the nonactive elements between the BARS and TINA, the so-called ''reconstructed energy'' for the RMC photon, was then computed. The energy deposited in the LST and the nonactive elements between the BARS and TINA was estimated using EGS (3) [39]. Our simulations indicated an estimated value for this energy was $\sim$2.5 MeV for a single electron and $\sim$5.0 MeV for two electrons[10] passing between the BARS and TINA.

D. Parameter estimation for the RMC photon neutral time spectrum

The background term: After the application of the cuts to the raw neutral data, the background was substantially reduced and appeared almost completely independent of time in the early-time window. Any structure that might have remained due to the cyclotron-related background was overshadowed by the Poisson uncertainty associated with the individual data points. Consequently, a constant background term, $B(t) \equiv B = \text{const}$, was chosen and its value was experimentally determined from a fit to the early-time region. This choice was later substantiated by scanning the neutral and the charged time spectra over time ranges greater than 43 ns to look for a possible periodicity in the observed asymmetry. None was found.

The precession frequency and the initial phase: Because of the abundance of the decay e^+ data and its associated large observed asymmetry, there is no depolarization of μ^+ within the target, the e^+ time spectrum was used for the precession frequency and the initial phase determination. The energy loss within the target due to interaction of the e^+ with the target material was also included. This was estimated from Monte Carlo simulation [EGS (3)] to be $\sim$7 MeV. From a χ^2 minimization of the e^+ time spectrum with a function of the form given by Eq. (5), it was possible to determine the precession frequency and the initial phase. To carry out these fits, the e^+ TDC spectrum was rebinned by a factor of 10. With our time calibration this meant a 10.11 ns time binning. Furthermore, the constancy of these fitted values were investigated by performing time and energy scans. Our average decay time for μ^+ from these fits was $\tau_{\mu^+} = 2.17 \pm 0.02$ μs [38] which agreed reasonably well with the present world average for the μ^+ lifetime of $\tau_{\mu^+} = 2.19703 \pm 0.0004$ μs [3]. The estimated value of the initial phase angle was $\varphi = 88.8° \pm 0.7°$, which also agreed quite well with the nominally expected value of 90°. The measured value of the precession frequency was $\nu = 5.50 \pm 0.01$ MHz, which is to be compared with the expected value of 5.50 MHz.

TABLE III. μ^--stop statistics for the RMC runs.

	$\langle p_{\mu^-} \rangle = 86$ MeV/c	$\langle p_{\mu^-} \rangle = 76$ MeV/c	Total statistics
$^{\#}\mu$ stops	7.37624×10^{10}	4.70885×10^{10}	12.08509×10^{10}

E. Extraction of the observed photon asymmetry, A_γ

The RMC asymmetry measurements were carried out at different average beam momenta: 76 and 86 MeV/c. Table III shows the total number of μ^- stops for each of these two cases.

With the limited number of candidate events available, an independent analysis for these two momenta was abandoned. Instead, all of the available data at both momenta were summed up to produce one neutral time spectrum. The observed photon asymmetry was then estimated by a fit to this time spectrum. Figure 5 shows the resulting time spectrum at

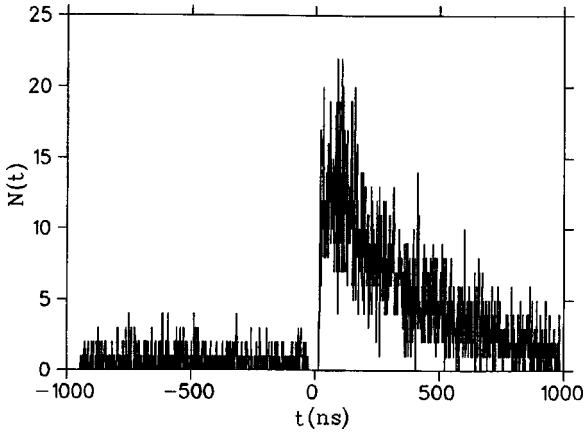

FIG. 5. Final neutral time spectrum shown at the raw TDC binning of 1.011 ns time bin. The plot shows both the background and the foreground time regions, which are separated by the prompt peak.

[10]These electrons were the result of photoconversion within the BARS.

TABLE IV. Optimization result for $E_{\max}$, which is the upper limit of the energy slice over which the observed photon asymmetry was estimated.

$E_{\max}$(MeV)	S_{86}	S_{76}	$S_{76}+S_{86}$
70.0	2395	1521	3916
75.0	2862	1785	4647
80.0	3094	1931	5025
85.0	3217	1989	5206
90.0	3249	2012	5261
95.0	3252	2019	5271
>95.0	3252±57	2019±45	5271±73[a]

[a]Our estimated data sample size based on this entry is 5200 high-energy event candidates.

1.01 ns/bin time binning after the application of all of the cuts.

For the neutral time spectrum, the integral signal (S) for the incident average beam momentum $\langle p_{\mu^-}\rangle$ was defined as

$$S_{\langle p_{\mu^-}\rangle}=\int_0^{960}\int_{\Delta E_\gamma} N(E_\gamma,t)\mathrm{dE}_\gamma \mathrm{dt}-\int_{-960}^{0} B(t)\mathrm{dt}$$

$$=\int_0^{960} N(t)\mathrm{dt}-\int_{-960}^{0} B(t)\mathrm{dt},$$

where ΔE_γ is the energy slice over which the observed photon asymmetry is defined. Since RMC was prominent for photon energies >57.0 MeV, the choice taken for the energy slice was $\Delta E_\gamma = E_{\max}-57.0$. The value of $E_{\max}$ was then chosen to maximize this signal. The results of these energy scans are presented in Table IV.

From Table IV it is seen that there is no gain in the RMC signal for $E_\gamma \geqslant 95.0$ MeV. The integral observed photon asymmetry was then appropriately estimated as

$$A_\gamma=\int_{E_\gamma\geqslant 57.0\ \mathrm{MeV}} A_\gamma(E_\gamma)\mathrm{dE}_\gamma=\int_{E_\gamma\geqslant 57.0\ \mathrm{MeV}}^{95.0} A_\gamma(E_\gamma)\mathrm{dE}_\gamma.$$

With the limited statistics in hand, a fit to the data at the best time binning of 1.011 ns/bin was impractical. In order to reduce the Poisson uncertainty associated with the individual data points used in the fit, it was necessary to rebin the data and fit at a coarser time binning. The resulting value of the observed photon asymmetry extracted from the neutral time spectrum was then attenuated somewhat by the angular averaging brought about by this rebinning of the data. If T_p is the precession period and T_b is the elementary bin time used in the fit ($[T_b]$ is the corresponding rebinning factor), this attenuation effect is expressible in terms of a reduction factor $r_{[T_b]}$. This reduction factor relates the true value of photon asymmetry A_γ to the estimated value of the attenuated observed photon asymmetry from a given fit, $A_\gamma^{([T_b])}$, according to the following equation:

$$A_\gamma=\frac{A_\gamma^{([T_b])}}{r_{[T_b]}}. \tag{6}$$

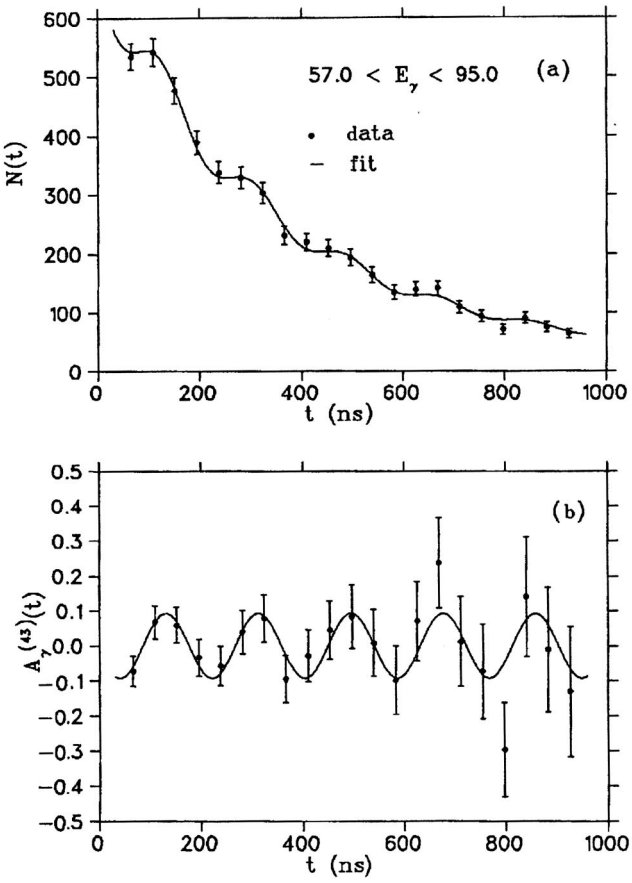

FIG. 6. Neutral time spectrum and its associated photon asymmetry displayed with a time binning of 43.47 ns and $t_1=25$ ns. Plot (a) shows the neutral time spectrum rebinned by 43 TDC bins. The fit includes a flat background term. In plot (b) the background and exponential decay terms have been subtracted to show the time-dependent photon asymmetry.

In this experiment, the precession frequency of 5.50 MHz corresponded to $T_p=181.8$ ns, resulting in $r_{[T_{10}]}=0.995$ for a 10-ns time bin and and $r_{[T_{43}]}=0.911$ for a 43-ns time bin.

In relation to our χ^2 minimization fit procedure, the following two ''constrained'' fit-types were employed.

(1) A ''semifree'' (SF) fit is one in which all of the parameters as per Eq. (5) except the background term are allowed to vary freely in the χ^2 minimization process.

(2) A ''partially restricted'' (PR) fit is one for which ω, φ, and B are fixed at their experimentally determined value[11] and τ is set to 333.0 ns [3].

Figure 6 shows the neutral time spectrum rebinned by a factor of 43 i.e., a time binning of 43.37 ns with its associated extracted and attenuated observed photon asymmetry. The corresponding plot at the higher time binning of 10.11 ns are shown in Fig. 7. In both cases, the fits shown are SF fits.

In order to demonstrate and validate the choice for a flat background, a time scan of the observed photon asymmetry

[11]Experimental values for ω, φ, and B were determined as described in Sec. IV D.

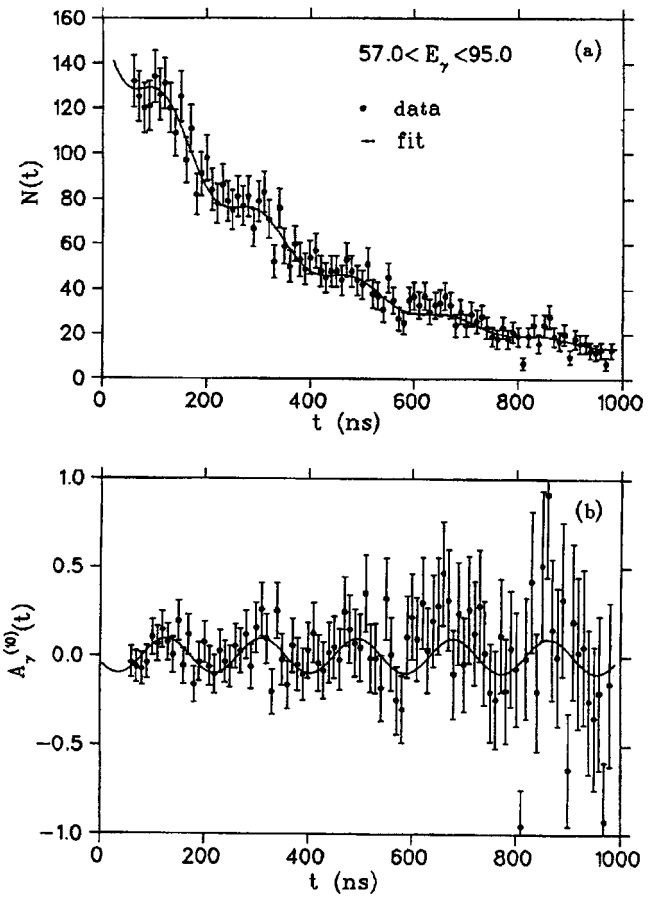

FIG. 7. Neutral time spectrum and its associated photon asymmetry displayed with a time binning of 10.11 ns and $t_1=25$ ns. Plot (a) shows the neutral time spectrum rebinned by 10 TDC bins. The fit includes a flat background term. In plot (b) the background and exponential decay terms have been subtracted to show the time-dependent photon asymmetry.

was carried out. The scan was sufficiently long to detect any possible periodicity existing in the time spectrum due to the 43.37 ns time structure associated with the cyclotron-related background [38]. Furthermore, it was necessary to ensure that rebinning by an arbitrary factor did not artificially affect the extracted value of the observed photon asymmetry, see Fig. 8. This was achieved by comparing results of time scans for two different rebinning factors: 43 and 10, where t_1 is the starting time for the fitting region. It is noted that with a rebinning factor of 43 (time binning of 43.47 ns), the background could be genuinely regarded as flat. This is due to the fact that our time binning of 43.47 ns matches closely the 43.37 ns cyclotron-related time structure. Table V and Fig. 8 present the results for the comparison of the two different rebinning factors. The fits are SF fits and they show the insensitivity of the extracted value of the observed photon asymmetry to the value of the rebinning factor.

Table VI presents the results of the PR and the SF fits to the neutral time spectrum for $t_1=25$ ns. The chosen value of the observed photon asymmetry is the one obtained from a PR fit to the neutral time spectrum with 43.47 ns time binning. The fitting region was chosen to have the smallest possible value of $t_1=25$ ns as this provided the largest number

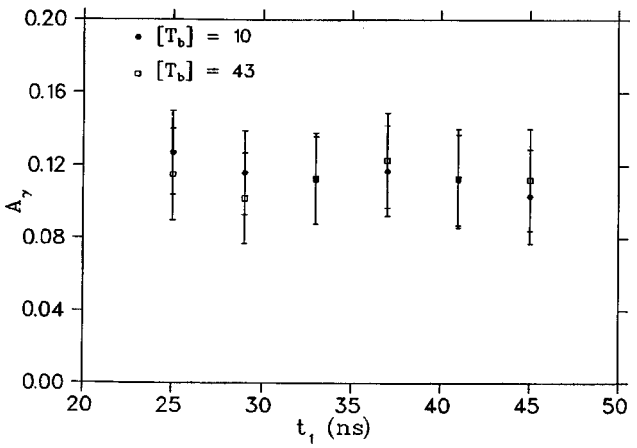

FIG. 8. Comparison of the time scans for the magnitude of the observed photon asymmetry with 43.47 ns and 10.11 ns time binnings.

of candidate events in our neutral time spectrum. Using Eq. (6) we get

$$A_\gamma=\frac{A_\gamma^{(43)}}{r_{[43]}}=\frac{0.1010\pm0.0213}{0.911}=0.111\pm0.023. \qquad (7)$$

F. Determination of physical photon asymmetry α_γ and extraction of g_P/g_A

By normalizing the value of the observed photon asymmetry to the μ^- residual polarization, $\langle P_{\mu^-}\rangle$ [32] our measured value of the physical photon asymmetry is determined to be

$$\alpha_\gamma=\frac{A_\gamma}{\langle P_{\mu^-}\rangle}=\frac{0.111\pm0.023}{0.111\pm0.010}=1.00\pm0.23.$$

Our chosen result for A_γ is based on a constrained fit with a $\chi^2_\nu=1.59$. The corresponding unconstrained fit (with $\chi^2_\nu=1.37$) provides a similar value. Furthermore, the unconstrained fit produces an acceptable value for the μ^- -decay lifetime in calcium of $\tau_{\mu^-}=(339\pm5)$ ns, and is able to "find" the asymmetry signal by reproducing the expected values for the initial phase and the precession frequency, given the statistical uncertainties associated with the data.

This measurement is an improvement of about a factor of 2 on the error associated with the value of the measured photon asymmetry compared to an earlier TRIUMF result of Virtue *et al.* [32].

Table VII presents the results of measurements of the photon asymmetry on ^{40}Ca. Our present value is in agreement with all the values except that reported by DiLella *et al.* [35]. DiLella *et al.* employed a bare NaI detector without any converters. Their estimated background due to the inclusion of the OMC neutrons was $\sim$45%. Their result is the only negative experimental value for the photon asymmetry and is in sharp disagreement with theories [28–30], which predict a large, positive photon asymmetry. To guard against such an OMC background, we employed an OMC neutron-

TABLE V. Table of the time scan for the observed photon asymmetry with 43.47 ns and 10.11 ns time binning and SF fits.

t_1 (ns)	$A_\gamma = \frac{A_\gamma^{(10)}}{r_{[10]}}$	χ_ν^2	$A_\gamma = \frac{A_\gamma^{(43)}}{r_{[43]}}$	χ_ν^2
25.0	$0.127(+0.02330/-0.0233)$	0.97	$0.155(+0.0247/-0.0246)$	1.37
29.0	$0.116(+0.0232/-0.0234)$	0.96	$0.102(+0.0247/-0.0246)$	1.46
33.0	$0.112(+0.0239/-0.0236)$	1.00	$0.113(+0.0248/-0.0252)$	1.39
37.0	$0.117(+0.0247/-0.0237)$	0.96	$0.123(+0.0260/-0.0259)$	0.74
41.0	$0.112(+0.0251/-0.0247)$	1.17	$0.113(+0.0265/-0.0263)$	0.74
45.0	$0.103(+0.0255/-0.0249)$	0.90	$0.112(+0.0277/-0.0275)$	0.59

discriminating capability in our setup by placing an active converter in front of our main NaI detector.

The result of Hart *et al.* [40] was obtained by a constrained fit ($\chi_\nu^2 \sim 1.0$) to their time spectrum containing $\sim$1200 events. With $\sim$30% energy resolution, they chose 63.5 MeV as their lower cutoff value for the RMC photon energy spectrum. From their e^- data, they obtained a value of $\tau_{\mu^-} = (366 \pm 8)$ ns, which is considerably larger than the presently accepted value of $\tau_{\mu^-} \sim 333$ ns [44]. Döbeli *et al.* [42] and Schaad [43] presented the results of the SIN/PSI group. They employed a pair spectrometer with the stroboscopic method. In this method, the muon precession frequency was tuned to that of the cyclotron frequency. The Schaad's value was extracted from a constrained fit to a time spectrum containing some 27 000 events. The authors did not quote χ_ν^2 for the final fit, but we estimate a value of $\chi_\nu^2 \sim 5$ from data, which implies that the quality of the fit is rather poor. Döbeli *et al.* [42] and Schaad [43] derived their model-dependent values of g_P based on Gmitro *et al.*'s modified impulse approximation (MIA) method [27]. The Schaad's value based on the photon asymmetry measurement is $g_P \approx (5.1 \pm {}^{4.4}_{7.0}) g_A$. Their results for g_P based on the rate measurement technique will be discussed in the following section.

The result of Virtue *et al.* [32] was obtained from an unconstrained fit ($\chi_\nu^2 = 1.10$) to a time spectrum containing 2500 events. Their value for $\tau_{\mu^-} = (352 \pm 4)$ ns is also larger than expected. Their final fit was chosen for $t_1 \geqslant 67$ ns to avoid the problematic early-time region in their time spectrum.[12] Due to their large value for the photon asymmetry, and its associated error, they could only quote an upper limit for the pseudoscalar coupling constant. Their results were $g_P < 5.2\ g_A$ for the traditional models and $g_P < 9.5\ g_A$ for the MIA model.

TABLE VI. Final PR and SF fits to the neutral time spectrum. The region of fit starts at $t_1 = 25$ ns with 43.47 ns time binning.

Type of fit	Parameter	Fitted value
PR	$A_\gamma^{(43)}$	0.101 ± 0.0213
	τ	333.0 (ns)
	ν	5.50 (MHz)
	φ	90 (degrees)
	χ_ν^2	1.59
SF	$A_\gamma^{(43)}$	$0.105\ (+0.0225/-0.0224)$
	τ	339.0 ± 5.1
	ν	5.57 ± 0.08 (MHz)
	φ	103 ± 11 (degrees)
	χ_ν^2	1.37

Figure 9 shows α_γ as a function of g_P/g_A for the Christillin's phenomenological model [25], Gmitro *et al.*'s IA model [26], and Gmitro *et al.*'s MIA model [27]. The MIA was introduced to remove the discrepancy between the photon yield as predicted by the phenomenological model of Christillin and the earlier IA model of Gmitro *et al.* The two traditional models seem to agree quite well, while the MIA is substantially different at higher g_P/g_A values—where it predicts a much smaller sensitivity of α_γ to g_P, and thereby indicating a significant model dependence in the theory. If we make a smooth fit to the theoretical data points of the traditional models of Christillin [25] and Gmitro *et al.* [26], we obtain the result $g_P/g_A < 8.0$. However, for the MIA model we obtain $g_P/g_A < 14.5$. Since the curves are rather flat the MIA value is nearly twice as large as the value obtained from the more traditional models. Unfortunately given the statistical uncertainly associated with our measurement and the theoretical discrepancy that exists between the MIA and traditional models does not allow us to constrain g_P effectively, so we will not try to draw any conclusions about its possible quenching inside nuclear matter. The current world average for the energy-averaged photon asymmetry $\alpha_\gamma = 0.98 \pm 0.15$—obtained as a weighted mean of the results of Hart *et al.* [40], Frischknecht *et al.* [41], Döbeli *et al.* [42], Virtue *et al.* [32], and our current measurement—is equally ineffective in this respect. The corresponding g_P/g_A extracted values based on the current world average for photon asymmetry measurement on ^{40}Ca are $g_P/g_A < 6.8$ for the IA model and $g_P/g_A < 12.0$ for the MIA model. It should be pointed out that the extraction of our energy-averaged photon asymmetry is weighted by the energy-dependence of the photon detection efficiency, while the theoretical results for IA and MIA are not. It has been assumed that this difference is small.

[12] Their extracted value of $A_\gamma(t_1 < 67$ ns) showed signs of systematic problems implying some distortion in their time spectrum for the early times, $t_1 < 67$ ns. It is noted that Hart *et al.* [40] were also forced to discard early-time data in the first 100 ns following a μ^- stop.

TABLE VII. Summary of photon asymmetry measurements on ^{40}Ca. The world average has been determined as the weighted mean of the entries in this table excluding the DiLella *et al.* and Schaad's results. The quoted χ^2_ν for Schaad's result has been estimated by us as the author has not provided a value for this parameter.

α_γ	χ^2_ν	No. of RMC photons	Reference
$<-0.32\pm0.48$	1.2	-	DiLella *et al.* 1971 [35]
0.90 ± 0.50	0.8	1 200	Hart *et al.* 1977 [40]
0.82 ± 0.76	-	1 900	Frischknecht *et al.* 1980 [41]
0.92 ± 0.26	2.7	7 000	Döbeli *et al.* 1986 [42]
0.94 ± 0.14	5.2[a]	27 000	Schaad 1983 [43]
$1.32\pm^{0.54}_{0.47}$	1.1	2 500	Virtue *et al.* 1990 [32]
1.00 ± 0.23	1.59	5 200	Present measurement
0.98 ± 0.15	N/A	N/A	The world average

[a]This is our estimated value for Schaad's χ^2_ν.

Finally, the question that one might now ask is, given the current theoretical uncertainties of α_γ dependency on g_P/g_A, could the photon asymmetry measurement technique with a sufficiently large data sample draw a definitive conclusion about g_P suppression within nuclear matter? To answer this question it is necessary to compare the degree of discrepancy in theory compared to our experimental uncertainty. From Fig. 9 it is seen that the IA model and MIA model predictions differ significantly, and, in fact, for the Goldberger-Trieman g_P/g_A value, the theoretical uncertainty for α_γ measured as the difference between the IA model and MIA model predictions is comparable to our experimental error. In the opinion of the authors, our ability to effectively constrain g_P and extract information about its renormalization within nuclear matter is currently limited by theory. What is now required are further theoretical investigations in order to resolve the discrepancy between the predictions of various nuclear models for RMC before any further improved experimental measurements are warranted.

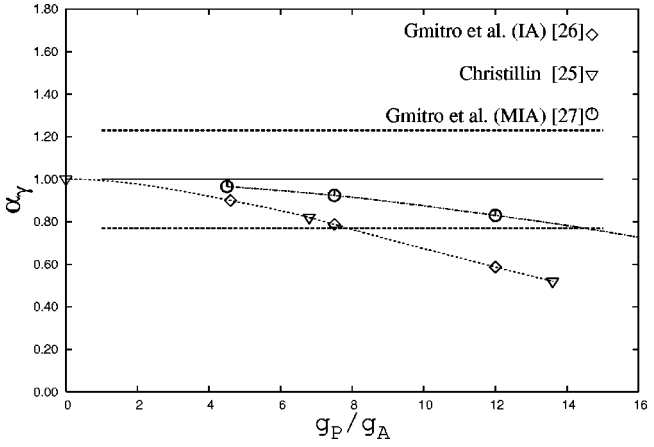

FIG. 9. Physical photon asymmetry as a function of the induced pseudoscalar coupling constant. The horizontal lines indicate our experimentally measured value with its associated errors.

V. DISCUSSION OF TRENDS IN g_P/g_A

In this section a summary of the g_P/g_A determination based on rate measurement techniques on medium to heavy nuclei is presented. For a good recent overview of the different theoretical as well as experimental aspects related to the determination of the induced pseudoscalar coupling constant of the weak interaction the reader is referred to Gorringe and Fearing [5]. It is noted that given the current status of RMC's theoretical and experimental techniques, the error estimate for g_P as determined by the photon asymmetry measurement technique is considerably larger than its counterpart obtained from the rate measurements on the same nucleus. The TRIUMF and the SIN results are both reviewed here.

The Virtue *et al.*'s [37] model-dependent value for g_P based on the rate measurement for ^{40}Ca utilizing the models of Christillin [25] and Gmitro *et al.* [27] is $g_P=(6.0\pm^{2.8}_{2.9})g_A$. Other TRIUMF rate measurements have been carried out for a number of different nuclei [45–47]. Their estimated value for ^{40}Ca [45] is $g_P=(4.6\pm1.8)g_A$. The SIN group have also presented results based on both the photon asymmetry measurement and the partial branching ratio measurement. They derive their model-dependent extracted values of g_P based on Gmitro *et al.*'s MIA method [27]. Döbeli et al. [48] reported their results for RMC rate measurements on several nuclei in the range $12<Z<83$—their value of g_P for ^{40}Ca is $g_P=(6.3\pm^{1.0}_{1.5})g_A$. A summary of g_P/g_A measurement on intermediate to heavy nuclei is shown in Table VIII [47].

The g_P/g_A results obtained from rate measurements, as seen in Table VIII, have been interpreted by others to indicate a general and gradual downward trend of g_P/g_A with increased nuclear charge for medium ($Z>20$) to heavy nuclei, well below the PCAC value, with full quenching of g_P at $Z\sim80$. This is in line with R_γ decreasing with Z. However, the authors feel that the interpretation of these results in terms of a Z-dependent quenching for g_P should be viewed with caution as there are still a number of significant outstanding theoretical issues.

(1) It has already been pointed out that although the general trends in g_P/g_A are reproducible, the extraction of ab-

TABLE VIII. Experimentally determined values for g_P/g_A based on integral rate measurement. The various theories have been abbreviated as follows: ''GKSO'' is Gmitro, Kamalov, Simlovic, and Ovchinnikova [27]; ''CG'' is Christillin and Gmitro [49]; ''GOT'' is Gmitro, Ovchinnikova, Tetereva [27]; ''RN'' is Roig and Navarro [50]; ''CSR'' is Christillin, Servadio, Rosa-Clot [51]; and ''C'' is Christillin [25].

Nucleus	Z	g_P/g_A	Theory	Experiment
C	6	$16.2\pm^{1.3}_{0.7}$	GKSO	[45]
O	8	13.5 ± 1.5	CG	[52]
		8.4 ± 1.9	CG	[48]
		7.3 ± 0.9	CG	[45]
		$13.6\pm^{1.6}_{1.9}$	GOT	[45]
		4.9 ± 0.5	CG	[47]
		$8.1\pm^{1.5}_{1.7}$	GOT	[47]
		$6.4\pm^{1.0}_{1.1}$	RN	[47]
Ca	20	4.6 ± 0.9	C	[53]
		6.5 ± 1.5	C	[37]
		$6.0\pm^{2.8}_{2.9}$	GOT	[37]
		5.9 ± 0.8	C	[46]
		5.0 ± 1.7	GOT	[46]
		7.8 ± 0.9	RN	[46]
		$6.3\pm^{1.0}_{1.5}$	C	[48]
		5.7 ± 0.8	C	[45]
		$4.6\pm^{1.7}_{1.8}$	GOT	[45]
Ti		<0	C	[47]
		<0	GOT	[47]
		$3.1\pm^{0.9}_{1.1}$	RN	[47]
Zr	40	$1.5\pm^{0.9}_{1.1}$	CSR	[47]
Mo	42	$0.0\pm^{1.6}_{4.1}$	CSR	[46]
Ag	47	2.2 ± 0.9	CSR	[47]
Sn	50	$0.1\pm^{1.4}_{7.5}$	CSR	[46]
Pb	82	<0.2	CSR	[46]

solute values are difficult. In Christillin's Fermi gas model [51], the observed decrease in g_P/g_A and R_γ with increase in Z occurs in terms of a quenching of g_P with Z. However, the g_P/g_A values to reproduce experimental R_γ's are in disagreement with the well-known OMC rates [44].

(2) Fearing and Welsh [54] have demonstrated that it is possible to reproduce the shapes of R_γ versus α plots[13] for $Z>20$ without requiring a Z-dependent quenching for g_P. Their estimated R_γ values are significantly larger (by a factor of ~ 2.5) than the experimental values using the PCAC value of g_P. They have also pointed out a sensitivity of R_γ to various inputs in Christillin's Fermi gas model [51], which makes the reliable extraction of g_P very difficult based on this model.

Hence the theoretical model-dependency is also a very major issue with regards to the rate measurement technique for extraction and interpretation of an absolute value for g_P.

[13]It is noted the α is neutron excess, which is not to be confused with RMC photon asymmetry α_γ.

VI. CONCLUSIONS AND FUTURE PROSPECTS FOR THE STUDY OF THE INDUCED PSEUDOSCALAR COUPLING CONSTANT

This paper has reported a TRIUMF measurement of the energy-averaged photon asymmetry in radiative muon capture on ^{40}Ca. Our measured value for this energy-averaged asymmetry utilizing our data sample size of 5200 candidate events is $\alpha_\gamma = 1.00 \pm 0.23$. The extracted values for the induced-pseudoscalar coupling constant g_P based on this measurement are $g_P/g_A < 8.0$ for the IA model, and $g_P/g_A < 14.5$ in terms of the MIA model. The two extracted values—although both consistent with the Goldberger-Treiman value of $g_P/g_A \approx 7$—are considerably different, indicating a significant theoretical model dependency.

Over the past three decades a very substantial effort has been invested both theoretically and experimentally in the OMC- and RMC-related techniques to gain further insight into the nature of nuclear matter by extracting and constraining the pseudoscalar coupling constant of the weak interactions, g_P. Although major advances have been made both theoretically and experimentally, many outstanding issues remain. One of the more surprising ones is that the value of g_P as determined from the RMC hydrogen data [18,19] is ~ 1.5 times larger than the PCAC prediction, while the value of g_P deduced from the OMC hydrogen data [17] is in good agreement with the PCAC prediction. Furthermore, this discrepancy cannot be explained by the higher order perturbation corrections within the context of the HBChPT [21]. The situation with regards to heavier nuclei is much more complicated due to additional nuclear interactions. The traditional models of Christillin [25], and Gmitro *et al.* [26] differ significantly from the more recent MIA [27] prediction, making the extraction and interpretation of g_P in terms of the photon asymmetry measurements very difficult. The rate measurements on medium to heavy nuclei have indicated a general and gradual decrease in the value of g_P/g_A with increased nuclear charge, well below the PCAC value. The interpretation of this observation in terms of Z-dependent quenching of g_P has been put inot question—Fearing and Welsh [54] have demonstrated that it is possible to reproduce the shapes of R_γ versus α plots—where α is neutron excess—for $Z>20$ without requiring a Z-dependent quenching for g_P. There is clearly a need for further theoretical investigations to resolve these major outstanding issues.

ACKNOWLEDGMENTS

The authors would like to thank and acknowledge the cumulative efforts invested by a number of people over the years in the RMC photon asymmetry measurement on calcium-40 experiments at TRIUMF (E47 and E364), notably, K. A. Aniol, F. E. Entezami, R. A. Burnham, and H. W. Roser. We also gratefully acknowledge the excellent experimental and programming facilities provided by TRIUMF. The research result reported here was supported in part by the Natural Sciences and Research Council of Canada (NSERC).

[1] M. Gell-Mann, Phys. Rev. **125**, 1067 (1962).
[2] N. Cabbibo, Phys. Rev. Lett. **10**, 531 (1963).
[3] K. Hagiwara *et al.*, Phys. Rev. D **66**, 010001 (2002).
[4] M.D. Goldberger and S.B. Treiman, Phys. Rev. **111**, 354 (1958); S.L. Adler and Y. Dothan, *ibid.* **151**, 1267 (1966).
[5] T. Gorringe and H. W. Fearing, Triumf Report TRI-PP-02-08, 2002.
[6] W. Weise, Nucl. Phys. **A396**, 373 (1983).
[7] M. Gell-Mann, Phys. Rev. **111**, 362 (1958).
[8] M. Morita, Hyperfine Interact. **21**, 143 (1985).
[9] B.R. Holstein, Phys. Rev. C **29**, 623 (1984).
[10] L.A. Ahrens *et al.*, Phys. Lett. B **202**, 284 (1988).
[11] V. Bernard *et al.*, Phys. Rev. Lett. **69**, 1877 (1992).
[12] S. Choi *et al.*, Phys. Rev. Lett. **71**, 3927 (1993).
[13] E. Jenkins and A.V. Manohar, Phys. Lett. B **255**, 558 (1991).
[14] V. Bernard *et al.*, Nucl. Phys. **B388**, 315 (1992).
[15] V. Bernard *et al.*, Phys. Rev. D **50**, 6899 (1994).
[16] H.W. Fearing *et al.*, Phys. Rev. D **56**, 1783 (1997).
[17] G. Bardin *et al.*, Phys. Lett. B **104**, 320 (1981); Nucl. Phys. **A352**, 365 (1981).
[18] G. Jonkmans *et al.*, Phys. Rev. Lett. **77**, 4512 (1996).
[19] D.H. Wright *et al.*, Phys. Rev. C **57**, 373 (1998).
[20] A. Ando and D.-P. Min, Phys. Lett. B **417**, 177 (1998).
[21] S. Ando *et al.*, Phys. Rev. C **65**, 015502 (2002).
[22] J.A. Wheeler, Rev. Mod. Phys. **21**, 133 (1949).
[23] L. Klieb, Ph.D. thesis, Groningen, 1982.
[24] L. Klieb and H.P.C. Rood, Phys. Rev. C **29**, 223 (1984).
[25] P. Christillin, Nucl. Phys. **A362**, 391 (1981).
[26] M. Gmitro, S.S. Kamalov, T.V. Moskalenko, and R.A. Eramzhyan, Czech. J. Phys., Sect. B **31**, 499 (1981).
[27] M. Gmitro, A.A. Ovchinnikova, and T.V. Tetereva, Nucl. Phys. **A453**, 685 (1986); M. Gmitro, S.S. Kamalov, and A.A. Ovchinnikova, *ibid.* **A468**, 404 (1987); M. Gmitro, S.S. Kamalov, F. Simlovic, and A.A. Ovchinnikova, *ibid.* **A507**, 707 (1990).
[28] H.P.C. Rood and H.A. Tolhoek, Nucl. Phys. **70**, 658 (1965).
[29] H.P.C. Rood, A.F. Yano, and F.B. Yano, Nucl. Phys. **A228**, 333 (1974).
[30] R.S. Sloboda and H.W. Fearing, Nucl. Phys. **A340**, 342 (1980).
[31] J. H. Brewer, K. M. Crowe, F. N. Gygax, and A. Schenck, *Muon Physics* (Academic press, New York, 1977), Vol. III.
[32] C.J. Virtue *et al.*, Nucl. Phys. **A517**, 509 (1990).
[33] A. Schenck, *Nuclear and Particle Physics Intermediate Energies* (Plenum Press, New York, 1976), p. 159.
[34] V.L. Highland, M. Salomon, M.D. Hasinoff, E. Mazzucato, D.F. Measday, J.-M. Poutissou, and T. Suzuki, Nucl. Phys. **A365**, 333 (1981).
[35] L. DiLella, I. Hammerman, and L.M. Rosenstein, Phys. Rev. Lett. **27**, 830 (1971).
[36] F. James and M. Ross, Comput. Phys. Commun. **10**, 343 (1975).
[37] C. J. Virtue, Ph.D. thesis, University of British Columbia, 1987.
[38] A. Pouladdej, M. Sc. thesis, University of British Columbia, 1987.
[39] R. L. Ford and W. R. Nelson, *The EGS Code System: Computer Programs for the Monte Carlo Simulation of Electromagnetic Cascade Showers (Version 3)* SLAC-210 (1978).
[40] R.D. Hart, C.R. Cox, G.W. Dodson, M. Eckhause, J.R. Kane, M.S. Pandey, A.M. Rushton, R.T. Siegel, and R.E. Welsh, Phys. Rev. Lett. **39**, 399 (1977).
[41] A. Frischknecht, P. Spierenburg, and W. Stehling, Helv. Phys. Acta **53**, 647 (1980).
[42] M. Döbeli *et al.*, Czech. J. Phys., Sect. B **36**, 386 (1986).
[43] M. Schaad, Ph.D. thesis, University of Zurich, 1983.
[44] T. Suzuki, D.F. Measday, and J.P. Roalsvig, Phys. Rev. C **35**, 2212 (1987).
[45] D.S. Armstrong *et al.*, Phys. Rev. C **43**, 1425 (1991).
[46] D.S. Armstrong *et al.*, Phys. Rev. C **46**, 1094 (1992).
[47] P.C. Bergbusch *et al.*, Phys. Rev. C **59**, 2853 (1999).
[48] M. Döbeli *et al.*, Phys. Rev. C **37**, 1633 (1988).
[49] P. Christillin and M. Gmitro, Phys. Lett. **150B**, 50 (1985).
[50] F. Roig and J. Navarro, Phys. Lett. B **236**, 393 (1990).
[51] P. Christillin, S. Servadio, and M. Rosa-Clot, Nucl. Phys. **A345**, 331 (1980).
[52] A. Frischknecht *et al.*, Phys. Rev. C **38**, 1996 (1988).
[53] A. Frischknecht *et al.*, Phys. Rev. C **32**, 1506 (1985).
[54] H.W. Fearing and M.S. Welsh, Phys. Rev. C **46**, 2077 (1992).